metals

MDPI

Article

Texture Development in Aluminum Alloys with High Magnesium Content

Evgenii Aryshenskii [1], Jurgen Hirsch [1,2], Alexander Drits [1,3], Sergey Konovalov [1,*], Vladimir Aryshenskii [1,3] and Maksim Tepterev [1,3]

[1] Department of Metals Technology and Aviation Materials, Samara National Research University, Moskovskoye Shosse 34, 443086 Samara, Russia; ar-evgenii@yandex.ru (E.A.); juergen.hirsch@hydro.com (J.H.); alexander.drits@arconic.com (A.D.); vladimir.aryshensky@arconic.com (V.A.); maksim.tepterev@arconic.com (M.T.)
[2] Research and Development, Hydro Aluminium Rolled Products GmbH, D-53117 Bonn, Germany
[3] Rolling Department, JSC "Arconic SMZ", Alma-Atinskaya 33/34, 443051 Samara, Russia
* Correspondence: ksv@ssau.ru; Tel.: +7-8462674640

Abstract: The evolution of texture in the $AlMg_6Mn_{0.7}$ (1565 ch) alloy throughout the entire cycle of its thermomechanical treatment has been studied. Using this alloy as an example, a new way is shown to control the texture development, which is applicable to alloys with high magnesium content. An integrated approach is applied, including optical and electron microscopy, as well as X-ray diffraction analysis, the determination of mechanical properties and texture modeling using algorithms of the crystallographic plasticity theory. All stages of the thermomechanical treatment have been studied, namely the development of the deformation structure out of the as-cast structure in the reversing hot-rolling stand, continuous hot rolling, cold rolling and final recrystallization annealing. The study showed that second phase particles are the main source of recrystallization nuclei at all stages of high temperature thermomechanical treatment. The importance of these particles increases when the Zener-Hollomon parameter increases. To obtain the maximum possible proportion of a random texture, thermomechanical processing must be carried out at high Zener-Hollomon parameters. However, the temperature should not interfere with the complete recrystallization process at the same time. After cold rolling and recrystallization annealing at temperatures equal or greater than 350 °C, a large proportion of random texture is formed, and the properties of the metal are almost isotropic.

Keywords: recrystallization; texture; microstructure; aluminum

Citation: Aryshenskii, E.; Hirsch, J.; Drits, A.; Konovalov, S.; Aryshenskii, V.; Tepterev, M. Texture Development in Aluminum Alloys with High Magnesium Content. *Metals* **2022**, *12*, 723. https://doi.org/10.3390/met12050723

Academic Editors: Angelo Fernando Padilha and Frank Czerwinski

Received: 14 March 2022
Accepted: 19 April 2022
Published: 24 April 2022

1. Introduction

Aluminum alloys with high magnesium content are one of the most widespread alloys in various branches of modern industry [1–6] due to their high strength and good plasticity characteristics. One of the problems arising during their production is the anisotropy of their physical and mechanical properties, which reduces their molding properties and performance and leads to metal losses [7–9]. The main reason for the anisotropy of mechanical properties is the crystallographic texture that develops during the thermomechanical processing of sheets and strips. The main way to reduce the anisotropy in deep drawing of a highly cold rolled sheet was to start with a hot strip that has a strong cube texture component giving 0°/90° ears that reduces the amount of rolling (β-fiber) textures which develop 45° ears in the final cold rolled state. As a result, the metal acquires properties close to isotropic [10,11]. In a fully recrystallized state, there is a different way to eliminate the anisotropy based on the recrystallization mechanism of particle stimulated nucleation "PSN" [12,13]. The PSN mechanism is based on the development of new recrystallization nuclei at intermetallic particles with more random orientations. As a result, recrystallization by the PSN mechanism does not lead to a pronounced texture. In some aluminum alloys with high magnesium content, the PSN mechanism during recrystallization can completely

prevail over other nucleation mechanisms in practically any modes of thermomechanical treatment [12,13]. This is facilitated, firstly, by the small subgrain size, which is characteristic of this alloy group [12–15], and, secondly, by the sufficiently large amount of Mn and Fe which contribute to the development of intermetallic compounds.

$AlMg_6Mn_{0.7}$ (1565 ch) is an alloy which can achieve a significant reduction in anisotropy using the PSN mechanism. Earlier studies showed the presence of a high number of large (greater than 1 microns) intermetallic particles in this alloy and small-sized subgrains [13]. Therefore, it can be assumed that under certain thermomechanical processing conditions, PSN will prevail over other recrystallization nucleation mechanisms, [13] generating a more random texture. The purpose of this study is to investigate the main feature of texture evolution in 1565 ch during thermomechanical treatments which allows us to decrease the anisotropy of mechanical properties. Additionally, it may demonstrate new ways of controlling texture formation using the PSN mechanism for aluminum alloys with high magnesium content.

2. Materials and Methods

Ingots of the $AlMg_6Mn_{0.7}$ (1565 ch) alloy with the chemical composition given in Table 1 were cast into a direct chill mold and homogenized at a temperature of 500–530 °C with a holding time of 4 h. The block diagram of thermomechanical processing is shown in Figure 1. It should be noted that this alloy is mainly used for various outer shells and structural parts in transport engineering. Hence, it is supplied in hot-rolled or fully annealed (after cold rolling) conditions.

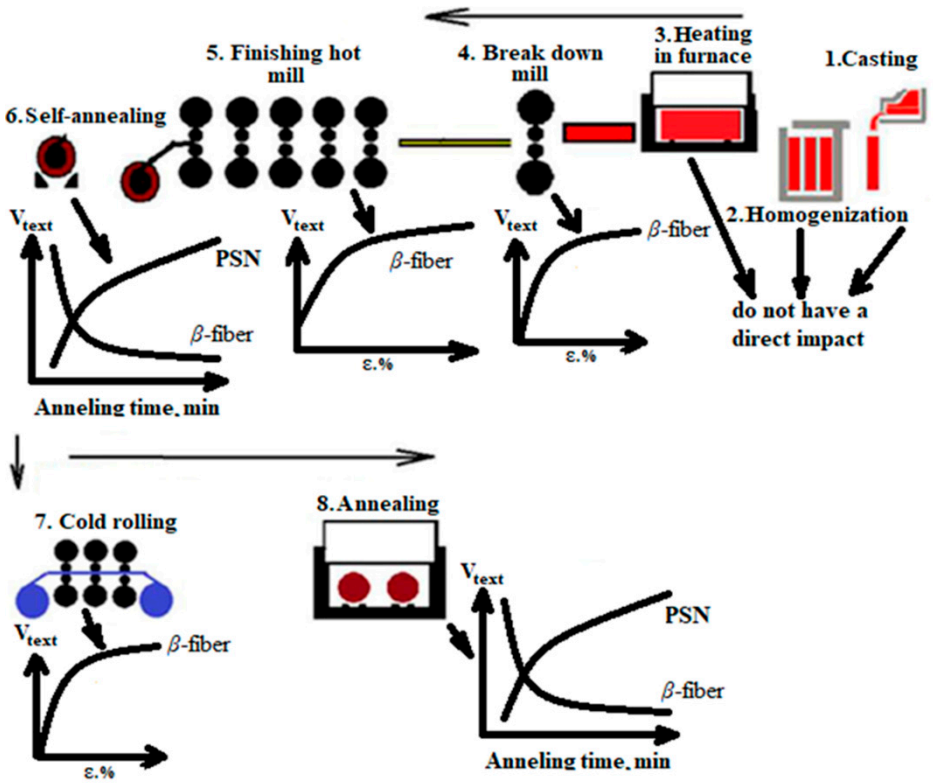

Figure 1. The main stages of thermomechanical treatment for the $AlMg_6Mn_{0.7}$ (1565 ch) alloy, including the features of changing the volume fraction of the main textural components.

Table 1. Chemical composition of the 1565 ch alloy ($AlMg_6Mn_{0.7}$).

Content of Chemical Elements, wt.%										
Alloy	Al	Si	Fe	Cu	Mn	Mg	Cr	Zn	Ti	Zr
1565 ch	base	0.12	0.22	0.05	0.80	5.6	0.06	0.50	0.07	0.10

As part of the study, industrial rolling of two cast billets from aluminum alloys with high magnesium content (1565 ch) was carried out in the reversing stand of a "Quarto 2800" hot rolling mill in order to study the evolution of the as-cast structure during hot-rolling according to the modes given in Table 2. After reverse hot rolling was completed, this batch of metal was cooled in air. Notably, its temperature was higher than the recrystallization temperature for several hours. The grain microstructure, size, number of intermetallic particles, as well as the texture composition were investigated.

Table 2. Rolling of the $AlMg_6Mn_{0.7}$ (1565 ch) alloy in the hot reversing mill.

Passnumber	Input Thickness, mm	Output Thickness, mm	Linear Speed of the Work Roll	Deformation Temperature, °C	Strain Rate, s^{-1}	Rolling Force, Tc	Zener Parameter Logarithm
1	400	390	57	460	0.35	2407	12.74
2	390	375	85	459	0.66	2350	13.03
3	375	355	85	459	0.79	2493	13.11
4	355	335	85	459	0.84	2432	13.13
5	335	310	85	459	0.99	2526	13.21
6	310	285	85	459	1.07	2447	13.24
7	285	255	85	459	1.28	2517	13.31
8	255	225	85	460	1.43	2436	13.35
9	225	190	85	460	1.74	2532	13.43
10	190	160	85	461	1.91	2325	13.46
11	160	130	85	460	2.26	2345	13.54
12	130	100	85	460	2.77	2457	13.63
13	100	75	85	460	3.28	2393	13.70
14	75	55	113	459	3.91	2351	13.80
15	55	40	113	455	6.15	2352	14.07
16	40	30	113	451	6.93	2233	14.19

Another part of the metal was sent to the continuous group of the "Quarto 2800" industrial mill (Figure 2). Hot rolling was carried out according to the modes given in Table 3.

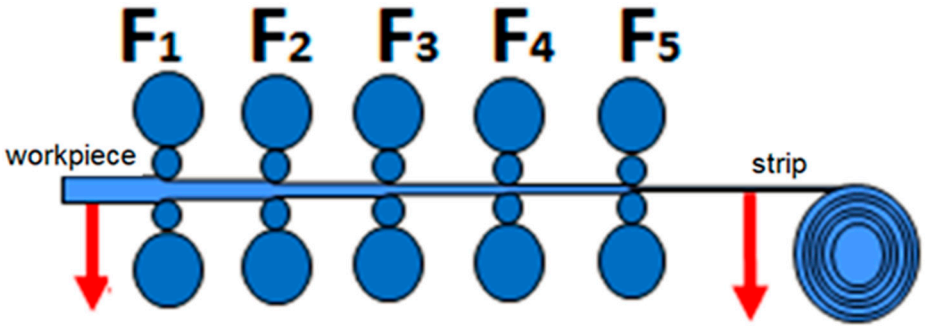

Figure 2. Layout of sampling from the continuous group of the "Quarto 2800" hot rolling mill.

Table 3. Rolling of the $AlMg_6Mn_{0.7}$ (1565 ch) alloy in the continuous group of the "Quarto 2800" mill.

Alloy	TMP Parameters	Entering a Continuous Group	Stand No F1	Stand No F2	Stand No F3	Stand No F4	Stand No F5
1565 ch	Thickness, mm	35	23	18	13.5	10	6.80
	Rolls rotation rate, m/min	-	33	48	65	92	128
	Temperature	460 °C	-	-	-	-	355 °C
	Interdeformation pause, s		10.9	6.4	4.1	2.433	-

During hot rolling, the process was stopped in the continuous group and the metal was efficiently cooled by the emulsion spray. Before and after each stand, samples were taken and prepared to determine the microstructure, texture, size and amount of the intermetallic particles. In addition, to study the structure and properties of the hot-rolled coil, a sample was taken after the fifth stand (at the exit from the mill) which was not subjected to sharp cooling but was cut out after the coil had been cooled in air. To exclude the effect of the surface friction on texture, the samples were cut from the middle of the hot-rolled billet.

After hot deformation in the continuous group, part of the metal was sent for cold rolling with 40–50% reduction and subsequent annealing at 250 °C, 350 °C and 500 °C. Afterwards, the intermetallic particles, their structure, texture and mechanical properties have been studied.

Texture measurements in the form of X-ray pole figures were carried out on the samples cut from the middle planes along the sheet thickness for each given state. The survey plane of the pole figures was parallel to the rolling plane. The texture in the form of three incomplete pole figures {111}, {200}, {220} was investigated by the "reflection" method using a DRON-7 X-ray diffractometer (Bourevestnik, Saint-Petersburg, Russia) in Cok_α radiation. The ranges of inclination α (0–70°) and rotation β (0–360°) angles with a step of α and $\beta = 5°$ were used. The drop in intensity on the peripheral part of the pole figure due to the defocusing effect was corrected using correction factors calculated based on the conditions of X-ray photography of pole figures. The orientation distribution function (ODF), representing a superposition of a large number (2000) of standard distributions with the same small scattering, was calculated from the measured pole figures. This ODF was also used to calculate the full pole figures and reverse pole figures for three mutually perpendicular directions in the sample: the normal direction (ND) to the rolling plane, the rolling direction (RD), and the transverse direction (TD).

The JEOL 6390A scanning electron microscope (JEOL Ltd., Tokyo, Japan) with the X-Max 80 energy dispersive detector (Oxford Instruments, Abingdon, UK) was used to determine the size and chemical composition of constituents and dispersed particles. The sample preparation technique consisted of mechanical grinding, polishing, and electropolishing. Electropolishing was carried out at 85–110 °C temperature and 10–30 V voltage in an electrolyte of the following composition: 500 mL of H_3PO_4; 300 mL of H_2SO_4; 50 g of CrO_3; and 50 mL of H_2O.

The grain size was determined on the Axiovert-40 MAT optical microscope (Carl Zeiss, Oberkochen, Germany) in polarized light (the samples were prepared by electropolishing in a fluor boron electrolyte) with the calculation of the average grain size by the secant method according to GOST 21073.

Mechanical properties (ultimate strength (σ_{max}), conventional yield strength ($\sigma_{0.2}$) and relative elongation (δ) were determined on flat specimens cut in three directions: along the rolling direction, transverse direction and at an angle of 45° to the rolling direction. To gather the statistics, five samples were taken for each direction. Tensile tests were carried out in accordance with GOST 1497 at the original gauge length 10 = 4b0 for 3104 and $10 = 5.65\sqrt{F0}$.

In addition, the texture and grain structure development was calculated at various stages of thermomechanical processing using the previously developed models [16–18].

3. Results

3.1. Evolution of Intermetallic Particles

After casting, large primary intermetallic compounds of the Al_6(FeMn)- and Mg_2Si-type (Figure 3a,c,d) with an average size of 10.3 μm and volume of 0.49% are developed in the $AlMg_6Mn_{0.7}$ (1565 ch) alloy. Intermetallic compounds of these two types are often found in aluminum alloys [19,20] with high magnesium content and were frequently observed in the present 1565 ch alloy [12,21]. The presence of Al_6(FeMn) is explained by the large amount of Mn as well as the presence of impurity iron (Fe) and silicon as (Mg_2Si)- due to the high content of magnesium (Mg) and some silicon (Si)-impurities. Both types of intermetallic compounds arise along the boundaries of dendritic grains. They are of eutectic origin with an elongated shape and small size (average radius of 1 μm). Finely dispersed particles (Figure 3b) are almost unobservable after casting.

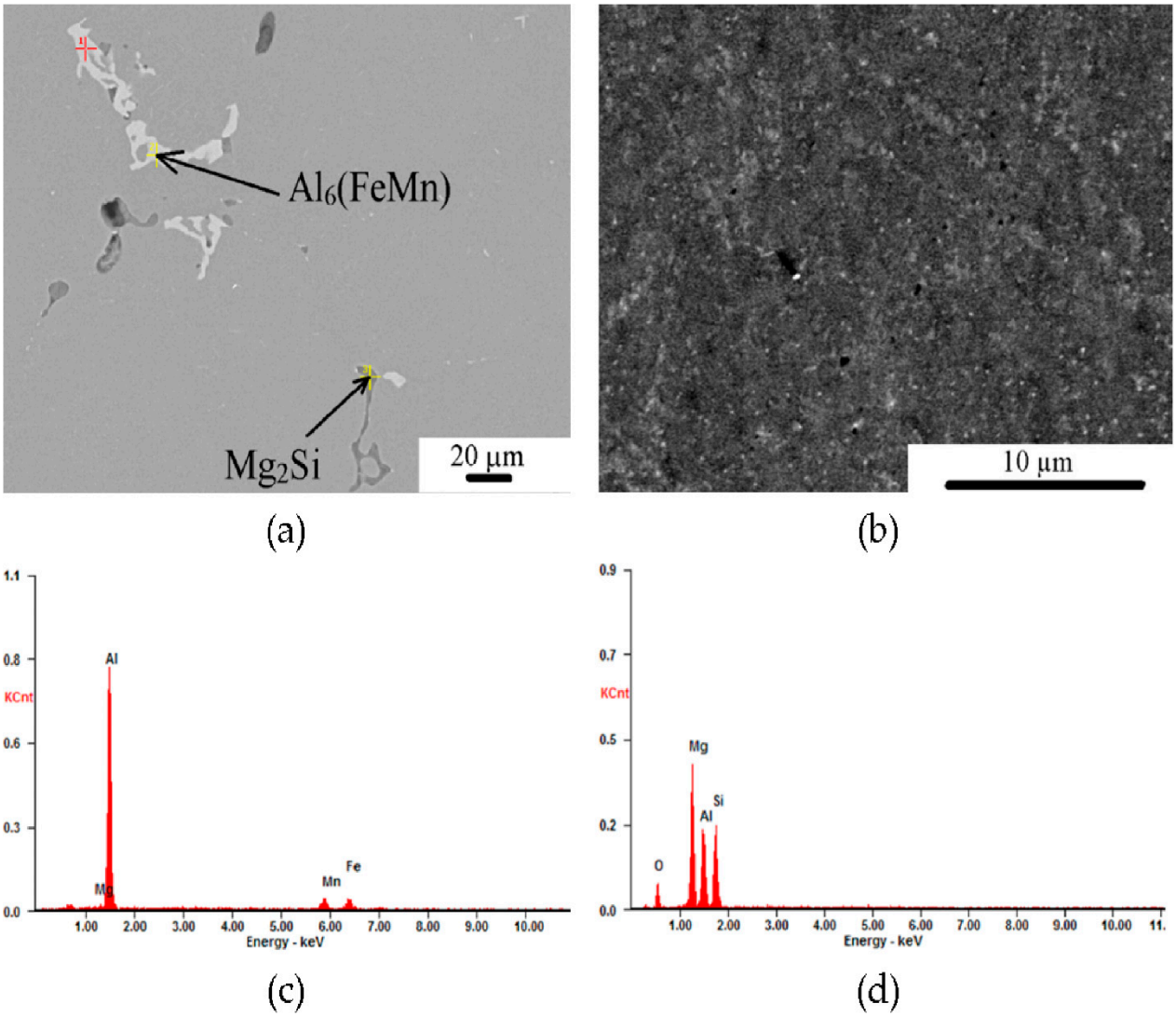

Figure 3. Second phase particles in the as-cast state of the 1565 ch alloy: (**a**) large 10.3 μm intermetallic compounds; (**b**) small 0.32 μm primary intermetallics; (**c**) EDS for Al_6(FeMn) particles; (**d**) EDS for Mg_2Siparticles.

After homogenization (Figure 4a), the average radius of large intermetallic compounds decreases to 8.66 μm, and their volume decreases to 0.33%. In general, there are many more large intermetallic particles in $AlMg_6Mn_{0.7}$ (1565 ch) as compared to other high-magnesium alloys.

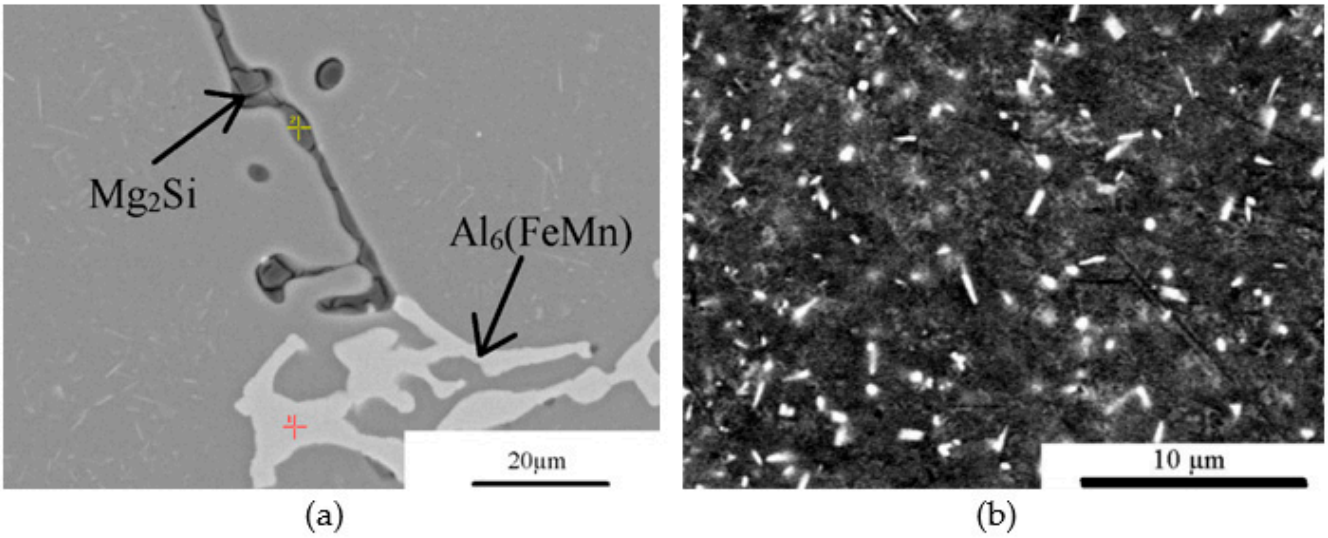

Figure 4. Second phase particles in the homogenized state of the 1565 ch alloy: (**a**) intermetallic compounds; (**b**) dispersoids.

At the same time, one can observe a large number of secondary phases as dispersoids (Figure 4b), which occupy more than 4.2% with a rather large average radius of 420 nm. The retarding force to grain boundary motion due to these particles (Zener dragPz) is 0.22 MPa, calculated according to Equation (1) [22]:

$$P_Z = \frac{3\gamma_B F_V}{r_D} \quad (1)$$

where F_V is the volume fraction of second phase particles; r_D is the average particle size.

It is not so high in comparison with other high-magnesium alloys. For example, the volume occupied by the particles in 5083 alloy is 1.04–1.3%; and their size is 22.9–51.2 nm [19]. In other aluminum magnesium 5754 the volume of intermetallic particles is 0.17% and their size is 126 nm. For both alloys the measurement was done in the homogenized state. As result, the retarding force in the 5083 alloy can reach 0.23–0.41 MPa depending on the homogenization mode [19]. Until the Zener drag Pz reaches 0.35 MPa, a completely recrystallized structure is observed, and when Pz becomes 0.41 MPa a partially recrystallized structure occurs. This suggests that recrystallization is also possible in the $AlMg_6Mn_{0.7}$ (1565 ch) alloy under certain conditions of thermomechanical treatment.

During the thermomechanical treatment of the as-cast structure in the hot reversing mill, the fragile eutectic intermetallic compounds are crushed (Figure 5a, Table 4), which has been repeatedly described in various studies [23–25]. As a result, their volume practically does not change. However, their number increases, facilitating the PSN mechanism. At the same time, no significant changes in the proportion of fine particles are observed. This is explained by the fact that the rolling process takes 8–10 min, which is not enough for the complete precipitation of fine metastable particles-in contrast to the homogenization process which lasts 4 h (Figure 5b).

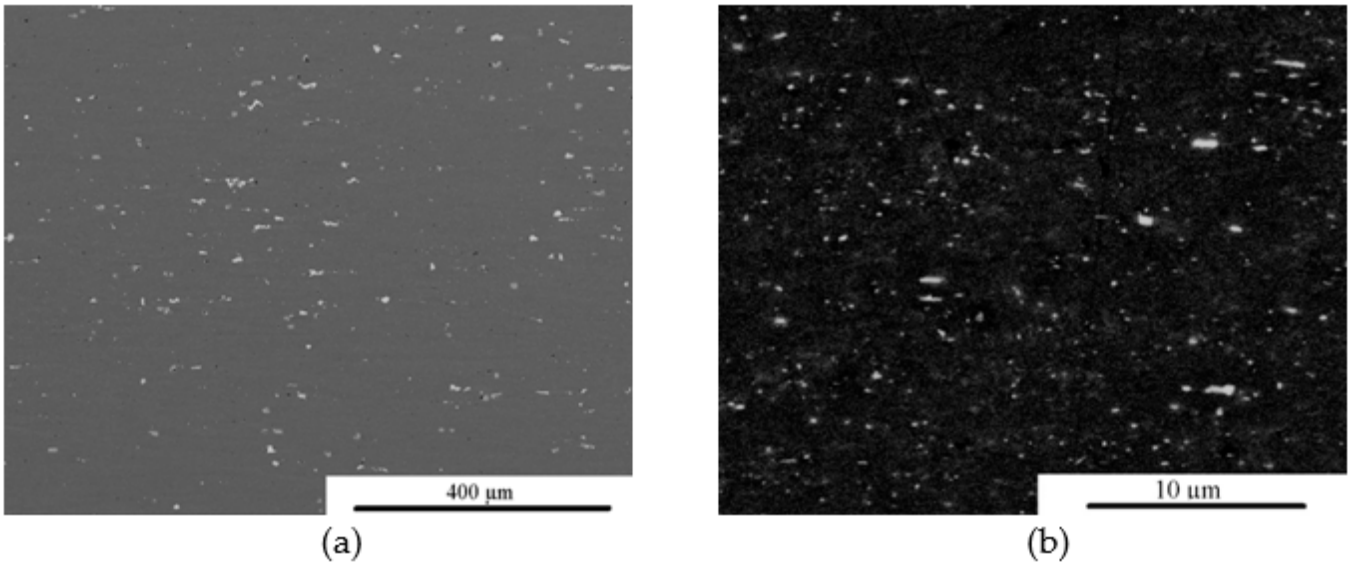

Figure 5. Second phase particles in the $AlMg_6Mn_{0.7}$ (1565 ch) alloy after hot deformation in the reversing stand: (**a**) intermetallic compounds; (**b**) dispersoids.

Table 4. Dimensions and volume fraction of intermetallic compounds in the $AlMg_6Mn_{0.7}$ (1565 ch) alloy.

Alloy	Sample Thickness, mm	Volume Fraction of Intermetallic Compounds, %	Average Diameter of Intermetallic Compounds, μm	Maximum Diameter of Intermetallic Compounds, μm	Volume Fraction of Dispersoids, 10^{-3}%	Average Diameter of Dispersoids, μm	Maximum Diameter of Dispersoids, μm
1565 ch	In-cast	4.9	10.3	13.96	-	-	-
	Hom.	3.3	8.66	9.9	8.2	0.42	0.48
	Reverse	3.2	6	6.52	8.4	0.4	0.45
	Continuous	3.0	5	5.38	8.7	0.33	0.38
	Coldrolled	2.2	2.5	5.22	10.7	0.51	0.58

During deformation in the continuous group of hot rolling stands, the intermetallic particles are barely affected, and their volume fraction, in general, does not change (Figure 6, Table 4). This result is consistent with the data obtained in [23], which also demonstrates that most active fragmentation of intermetallic compounds occurs in the break-down hot mill at the early stage of hot working of the as-cast structure. After that, the tendency to fracture and further fragment decreases. This evolution of particles is due to the initial crushing of the most fragile intermetallic compounds which are represented by nonequilibrium eutectics that survived the homogenization process. Harder and finer-sized intermetallic compounds, close to the equilibrium phase, are not so prone to crushing at any stage of thermomechanical treatment. Also, the size and amount of fine particles is stable. Hence, changes in the size and amount of intermetallic particles are insignificant and cannot affect the recrystallization process at this stage.

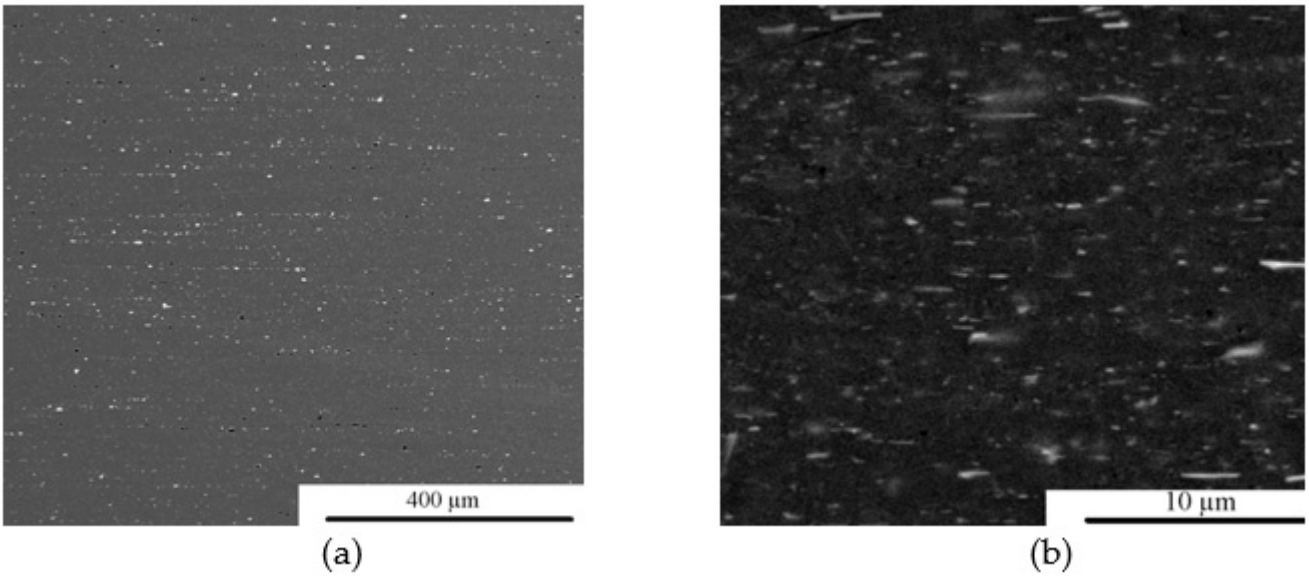

Figure 6. The $AlMg_6Mn_{0.7}$ (1565 ch) particles after hot deformation in the continuous group: (**a**) intermetallic compounds; (**b**) dispersoids.

In the case of cold rolling, the average size of the intermetallic compounds is cut in half in comparison with the hot-rolled state (Figure 7a, Table 4). This suggests that these particles begin to crush again during cold deformation. A possible explanation for this pattern observed in this alloy is that the aluminum surrounding these particles has a significantly higher strength during cold deformation. Therefore, the force on the intermetallic particles, which contributes to their fragmentation, increases and can have a double effect on the PSN-mechanism. On one hand, it increases the number of potential locations where PSN nuclei can arise on the second phase particles. On the other hand, it reduces the probability of their further growth since the size of potential PSN nuclei is significantly reduced.

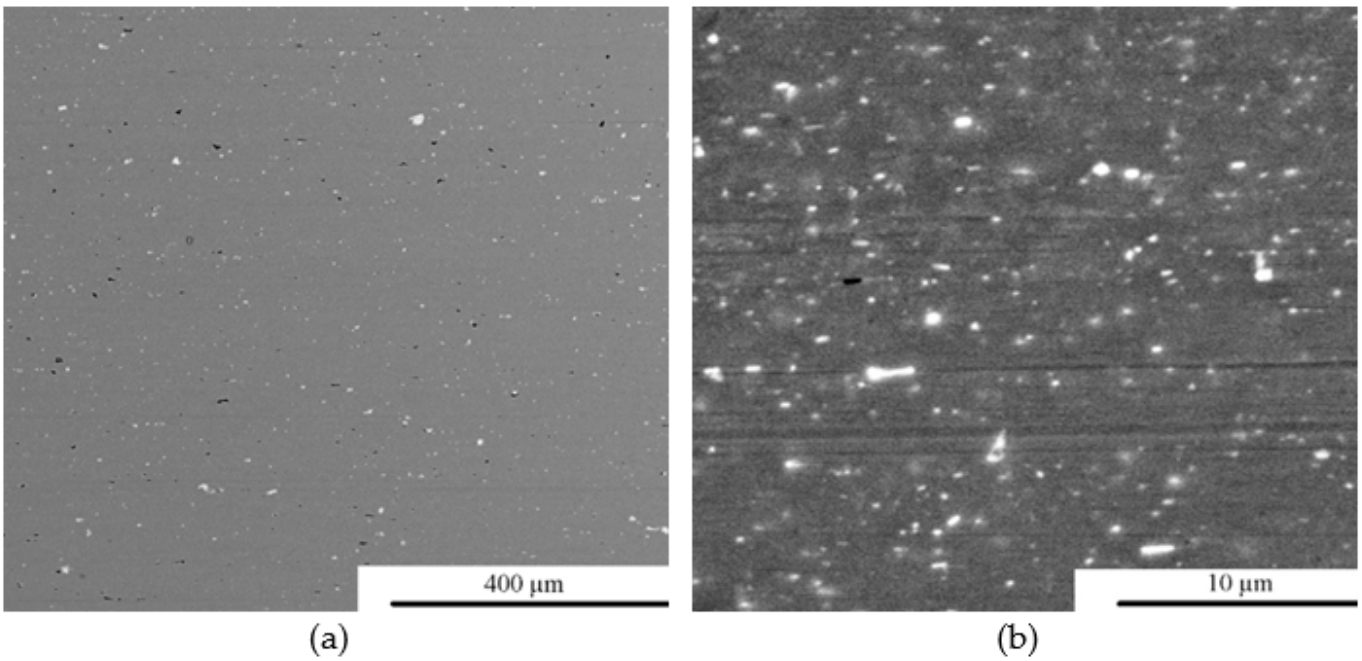

Figure 7. The $AlMg_6Mn_{0.7}$ (1565 ch) particles after cold deformation, sheet thickness 5 mm: (**a**) intermetallic compounds; (**b**) dispersoids.

In addition, the size and number of fine particles increases (Figure 7b, Table 4). This also has a double effect on the recrystallization pattern. On the one hand, an increase in their number will contribute to its inhibition. On the other hand, an increase in their size will lead to the opposite effect.

After annealing at 250 °C (Figure 8a), the amount of intermetallic particles generally does not change compared to the cold rolled state. Both Al_6(FeMn) and Mg_2Si particles are present in the alloy. At the temperature of 350 °C (Figure 8b), the number of intermetallic compounds of the Mg_2Si type is somewhat decreased. At the same time the amount of Al_6(FeMn) remains unchanged. This is explained by the fact that the dissolution temperature of Al_6(FeMn) is more than 50 °C higher than Mg_2Si [19]. It should be noted that the dissolution of the Mg_2Si in our case occurs at lower temperatures than the calculations done in ref. [19] predict. This could be explained by the fact that the computation was carried out for the precipitation of fine particles, while in this case, Mg_2Si compounds have a much more nonequilibrium nature and were formed during crystallization. Their rapid dissolution precisely at this stage of thermomechanical treatment can also be explained by the fact that after cold rolling their size is significantly reduced, which makes their dissolution easier. Heating at a temperature of 500 °C (Figure 8c) leads to a further decrease in the amount of Mg_2Si particles.

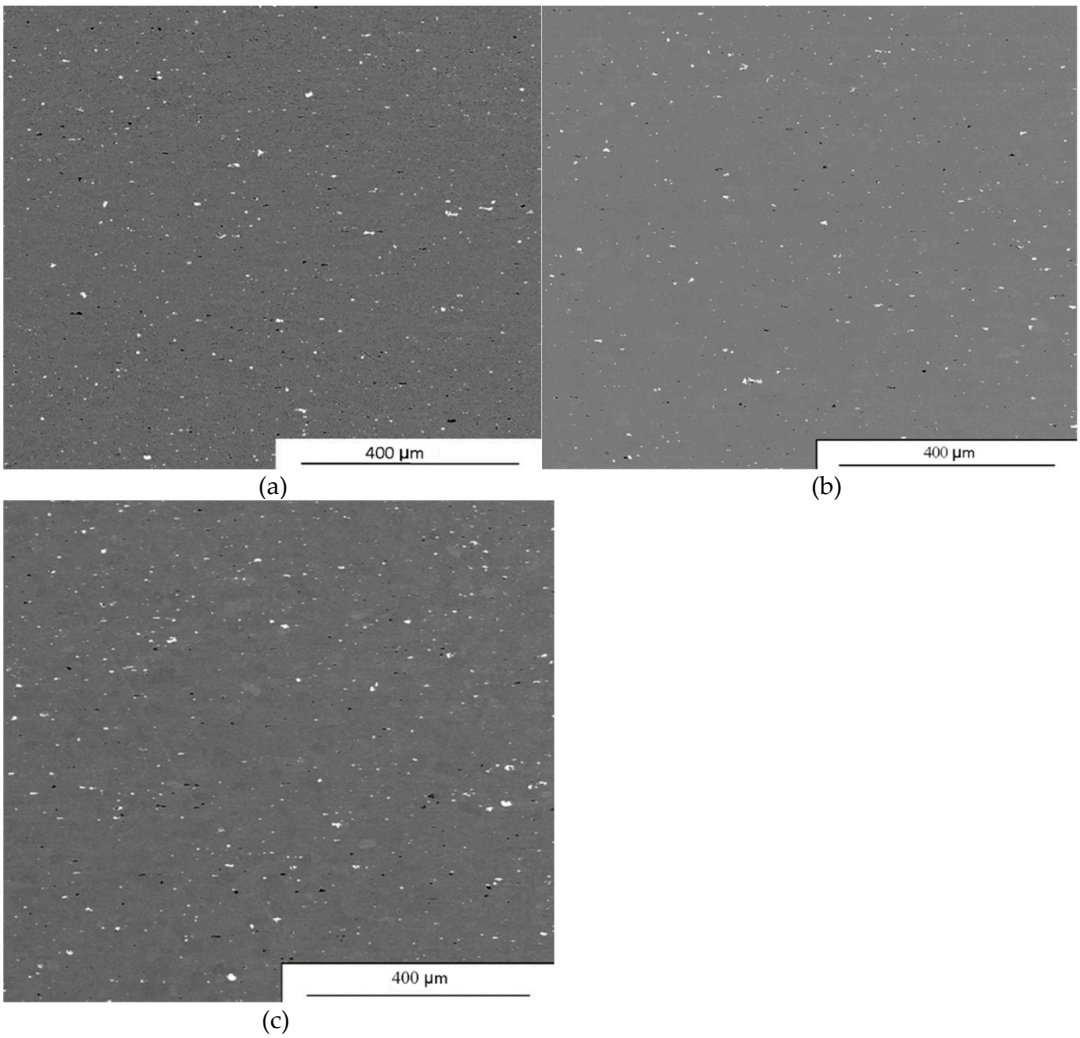

Figure 8. Intermetallic compounds after annealing (**a**) 250 °C, (**b**) 350 °C and (**c**) 500 °C.

Fine particles behave in a similar manner as large ones. At the temperature of 250 °C (Figure 9a, a large number of dark fine particles that can be attributed to Mg_2Si, as well

as the light dispersoids of the Al6(FeMn) type. When heated to 350 °C (Figure 9b), Mg_2Si dispersoids actively dissolve, and at 500 °C (Figure 9c) they completely disappear. At the same time, an increase in temperature does not affect the number and size of light particles of the Al_6(FeMn) type. It should be noted that Mg_2Si dissolve even faster than large non-equilibrium intermetallic compounds of the same type. This may be explained by the fact that fine particles are usually much smaller in size (>1 μm) and therefore dissolve faster. Additionally, it is impossible to accurately determine the composition of small dispersoids by using SEM. As a result, it can be both Mg_2Si as well as the much less stable β(Al_3Mg_2) particles [19]. The latter might precipitate at the end of self-annealing when the temperature becomes less than 250 °C [19].

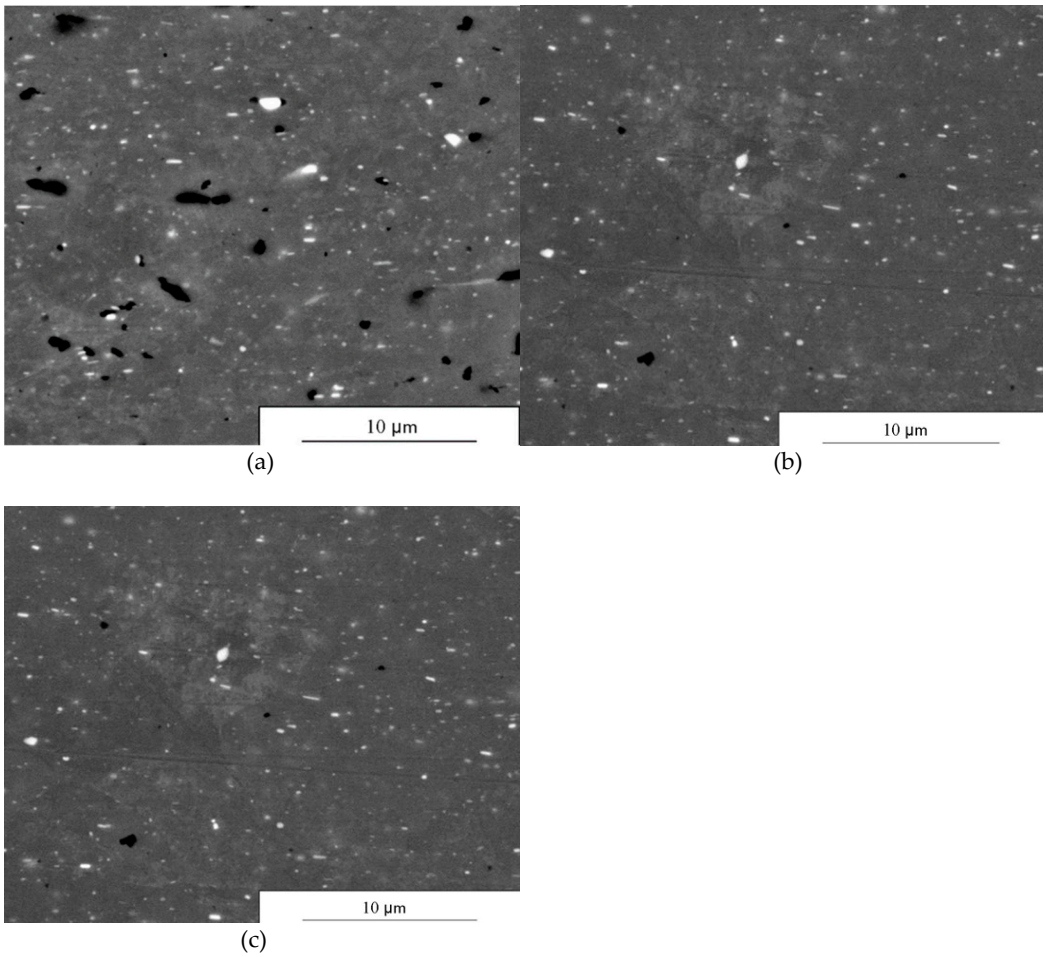

Figure 9. Dispersoids after annealing (**a**) 250 °C, (**b**) 350 °C and (**c**) 500 °C.

3.2. Grain Structure Evolution

In the as-cast state the alloy1565 ch has a dendritic structure, with 350 μm average grain size. A deformed structure with elongated grains and small inclusions of equiaxed recrystallized grains is observed in the investigated alloy (Figure 10). The main reason for this is the observed fine intermetallic particles (dispersoids) which inhibit the recrystallization process. This is due to the low Zener-Hollomon parameter at this stage of thermomechanical treatment, where the energy accumulated during deformation is insufficient for recrystallization to occur. The development of the small recrystallized fraction can be explained by the large second phase intermetallic particles which accumulate more dislocations around them than other elements of the microstructure [26]. Therefore, the recrystallization nuclei formed around them require much less Zener-Hollomon energy to start the recrystallization process. However, due to the fine particles, the subsequent

motion of the high-angle boundaries is blocked when they move out of the area with high dislocation densities accumulated around the particle.

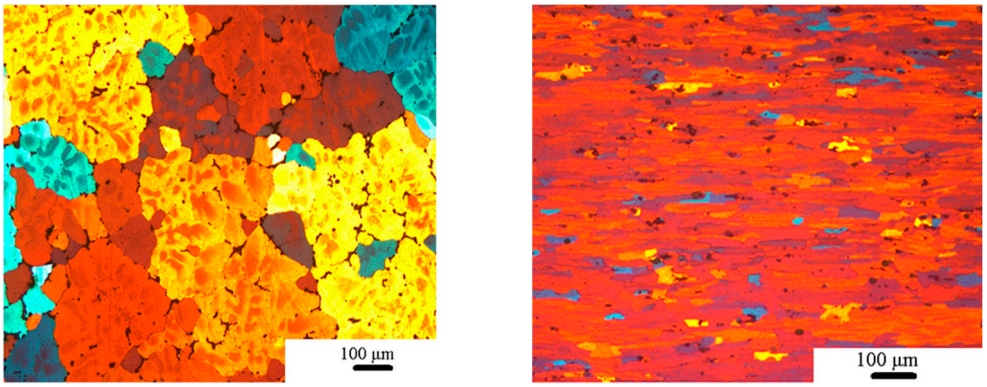

(**a**) (**b**)

Figure 10. Results of Al $Mg_{4.5}Mn_{0.3}$ (AA5182) and$AlMg_6Mn_{0.7}$ (1565 ch) alloys optical microscopy results of the as-cast structure (**a**) and after reversing mill (**b**).

When the $AlMg_6Mn_{0.7}$ (1565 ch) alloy is hot rolled in the continuous group with five stands there is almost no recrystallization between the deformation steps (Figure 11b,c). This is due to the fact that the time between the deformation pauses is very short. Therefore, despite the higher Zener-Hollomon parameter, recrystallization does not have time to occur in contrast to the alloys 5182 [27] (and 3104 to some extent). This difference in the recrystallization kinetics is explained by the fact that there are many fine intermetallic particles in this alloy that hinder grain boundary motion, as mentioned above. However, the recrystallization process proceeds completely during subsequent self-annealing in the hot coil. This can be attributed to two factors: The first is the high Zener-Hollomon parameter, which reaches its maximum value at the output of the last hot rolling stand. This, in turn, leads to a significant increase in the recrystallization driving force which overcomes the retarding effect of fine particles. Another factor contributing to recrystallization is the time required for it to occur (several hours during coil cooling in comparison with 5–10 s in inter-stand deformation pauses).

After cold rolling (Figure 12a), grains are elongated in the rolling direction, i.e., a typical deformed structure develops. When heated to 250 °C (Figure 12b), the deformed grains elongated in the rolling direction are still observed. When heated to 350 °C temperature (Figure 12c), complete recrystallization with a new fine-grained structure (an average size of 21 μm) is observed. When the temperature of recrystallizing annealing is increased to 500 °C (Figure 12d), the grain structure, in general, does not change its size. Thus, the recrystallization process proceeds completely in the cold-rolled state after annealing at a temperature equal to or greater than 350 °C. It is facilitated by the accumulated internal energy of structural imperfections, which is much higher than at the hot rolling stage. Moreover, there is enough time to fully complete the recrystallization process.

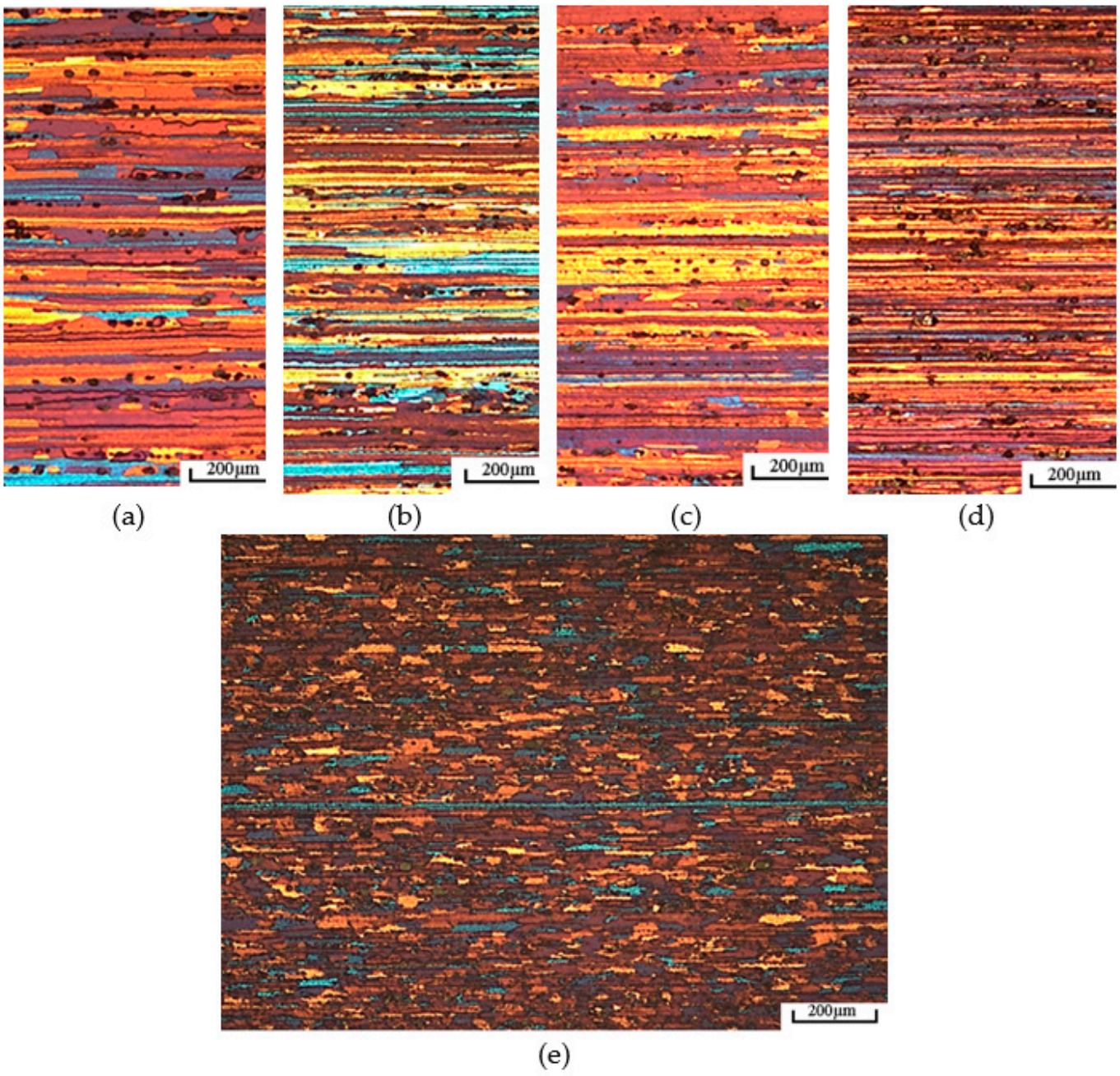

Figure 11. Change in the microstructure of the Al Mg6 Mn0.7 (1565 ch) strip during hot rolling in the continuous hot rolling group. Longitudinal section. 200:1 scale: (**a**) before F1; (**b**) after F1; (**c**) before F2; (**d**) after F5, (**e**) after hot rolling with slow cooling.

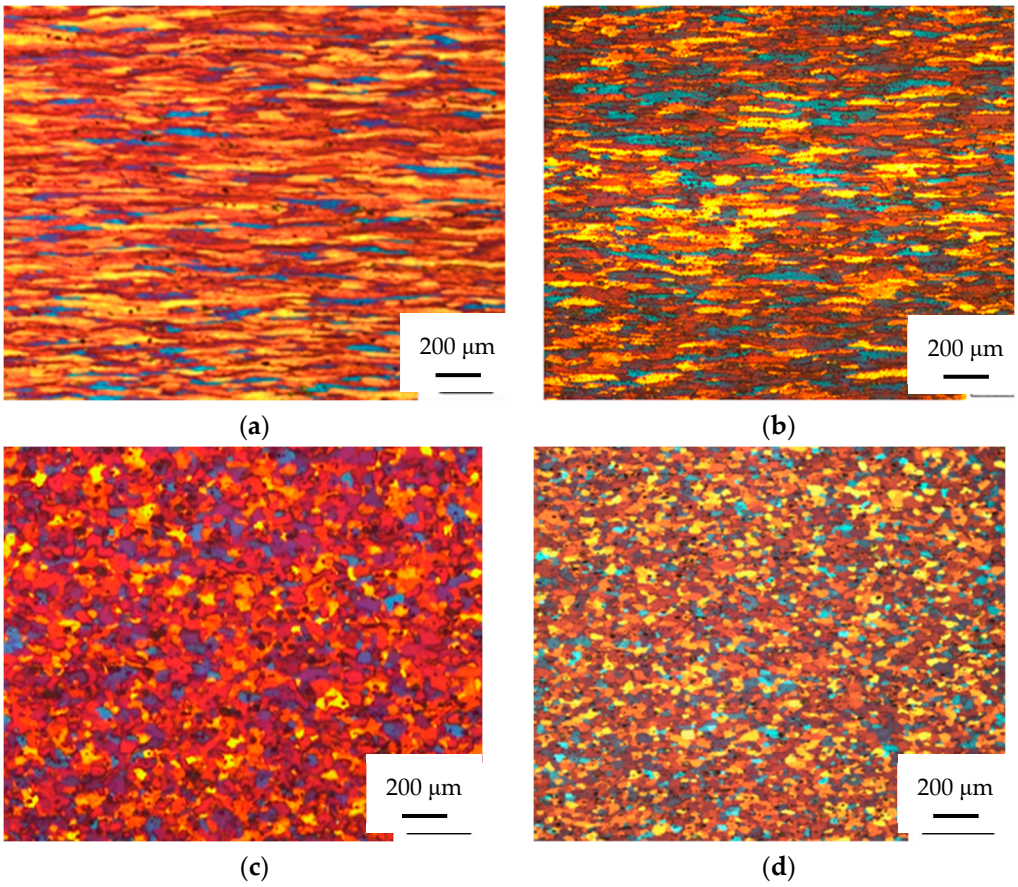

Figure 12. Grain structure after annealing of cold-rolled sheet (**a**) after cold rolling (**b**) after annealing at 250 °C, (**c**) after annealing at 350 °C, (**d**) after annealing at 500 °C.

3.3. Texture Evolution

The $AlMg_6Mn_{0.7}$ (1565 ch) alloy does not have a pronounced texture (Figure 13a) in the as-cast state, which is a standard scenario for this casting method [28]. After the cast structure is processed in the hot-reversing stand, a rolling (β-fiber) texture is observed, expressed mainly by the brass "Bs" component (Figure 13b). For a better understanding of the main features of texture evolution at the early stage of thermomechanical processing, we consider the results of the calculated rolling texture evolution.

The orientation distribution pattern (texture) after deformation in the first stand (Figure 14a) is generally similar to the one observed after the processing of the cast structure (Figure 14b). The main dominant texture component is the brass "Bs" component. As noted earlier, deformation along the two slip planes of this component with the lowest Taylor factor [29] is most beneficial in alloys with high magnesium content, and the hardening on it is less than in other alloys of this system [18]. The S-component characteristic of aluminum alloys is formed in addition to the brass-type texture during further deformation in the five-stand group. This is due to the fact that no softening occurs in inter-deformation pauses and the systems of planes associated with the Bs-component are gradually blocked. Note that the "S-type" texture component {124}<211>appears faster in other aluminum alloys. The Cu-texture component {112}<111> does not appear in the $AlMg_6Mn_{0.7}$ (1565 ch) alloy even during deformation in the last stand. An insignificant cubic texture is observed after self-annealing and other pronounced texture components are not observed.

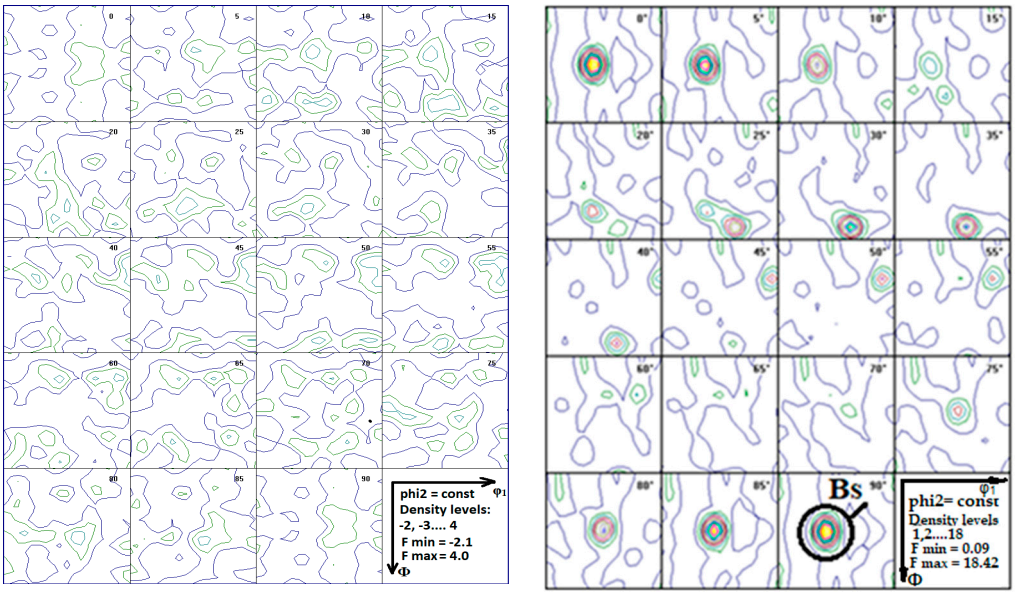

(**a**) (**b**)

Figure 13. Texture composition for the $AlMg_6Mn_{0.7}$ (1565 ch) alloy: (**a**) cast state, (**b**) after the reversing stand.

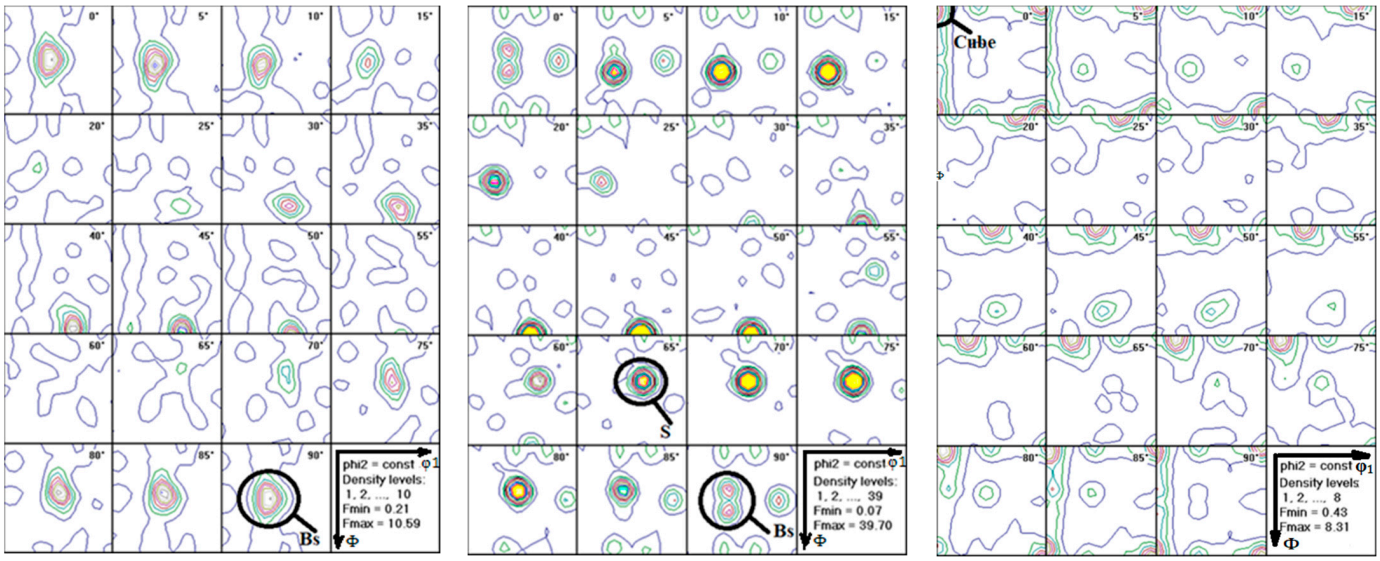

(**a**) (**b**) (**c**)

Figure 14. Results of X-ray structural analysis (ODF data). (**a**) before the second stand, (**b**) after the fifth stand, (**c**) after self-annealing.

As can be seen from the ODF data analysis, a stable rolling texture (β-fiber) consisting mainly of the classical S-component as well as a small amount of Cu-(copper) and Bs-(brass) textures is formed as the deformation proceeds. The transition of these components into the recrystallization textures during inter-deformation pauses cannot be observed, despite the rather long time available for their development. This strongly distinguishes this alloy from the classical 5182 in which recrystallization textures are intensely formed during inter-deformation pauses [30,31]. The difference can be explained by the large number of dispersoid particles formed due to zirconium, which is poorly soluble in aluminum. These particles can significantly reduce the growth rate of new grain boundaries. At the same time, the deformation textures partially transform into recrystallization textures during

self-annealing. However, they transform into a "textureless" (random) component. This can also be explained by an increased content of manganese in the form of intermetallic particles which generate the PSN random texture component [32]. Thus, it can be concluded that the alloy is not prone to the formation of a pronounced recrystallization texture but the proportion of the random component is quite large at all stages of hot rolling. Therefore, the hot-rolled sheet shows a weak anisotropy of properties. However, in the case of subsequent cold rolling, a sharp deformation texture will still be formed which will lead to a sharp increase in anisotropy, which can hardly be compensated for by an initial cube recrystallization texture component, as done in can stock.

In the texture of the sample annealed at 250 °C (see ODF in Figure 15), the classical texture of β-fiber of rolled aluminum alloys develops during deformation [33]. It starts with the brass texture which lies in the center of the φ_2 = 90° (equivalent to φ_2 = 0°) section, usually denoted as the Bs component. Orientations close to Bs along the β-fiber are observed in the φ_2 = sections lower than 90° down to φ_2 = 65° (S). The Cu (copper) component occurs in the φ_2 = 45° section and expands along the ß-fiber up to φ_2 = 65° (S). In general, this is a classical picture inherent in cold-worked aluminum alloys [33–35] with a predominance of the Bs-texture, characteristic of aluminum alloys with high magnesium content [18]. The data of X-ray structural analysis are confirmed by the data of optical metallography, showing the absence of recrystallization at 250 °C. It is worth noting that there is a fraction of the cube texture and components close to it which are located in all φ_2 sections of the ODF figure. However, the cube texture component is still rather weak. It should be noted that this component is retained in a sufficient volume upon annealing after a 50% reduction in high magnesium aluminium alloys [34,35]. The pattern observed in Figure 15 can be explained by the fact that the cube texture is almost not observed in the hot-rolled state after self-annealing as well, which explains its small fraction at the next stages of heat treatment.

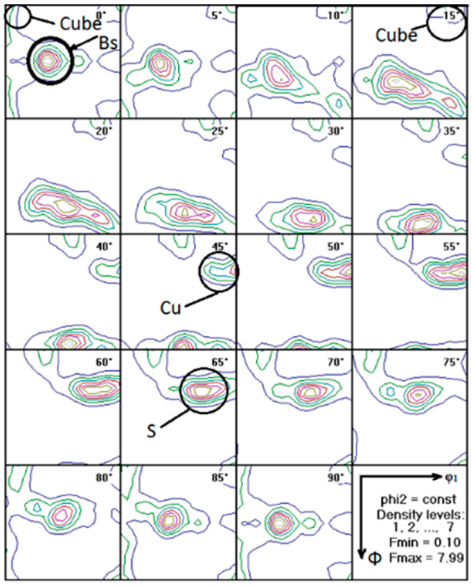

Figure 15. ODF for the state after annealing at 250 °C with a 3-h exposure.

ODFs for annealing at 350 °C (Figure 16a) and 500 °C (Figure 16b) are shown in one figure on purpose, since the observed texture compositions almost coincide. Except for the sections from φ_2 = 85° to φ_2 = 90°, where the texture of brass Bs and texture components close to it are observed, there are no other pronounced components. One can hardly observe the cube texture component. In general, the texture is similar to that observed for this alloy in the hot-rolled state after self-annealing [36]. The presence of the Bs texture can be explained by the fact that after annealing some unrecrystallized (highly recovered) grains

(which remain undetected by optical microscopy) contain these components. It must be mentioned that Bs has more resistivity to recrystallization, so they have more chances to survive [37].

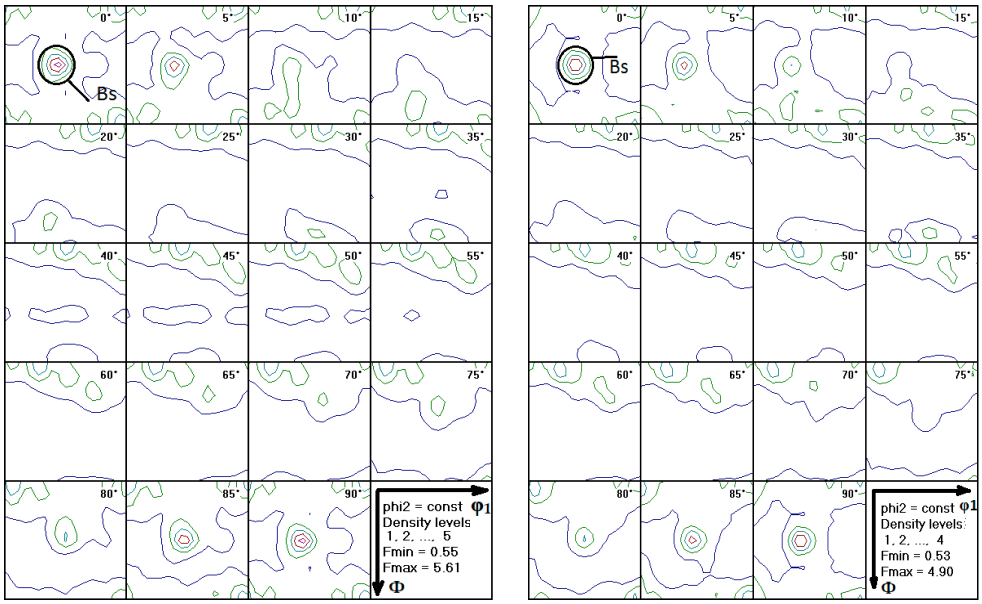

(**a**) (**b**)

Figure 16. ODF for the state after annealing, (**a**) 350 °C and (**b**) 500 °C with 1-h exposure.

After cold rolling and annealing at 500 °C, the $AlMg_6Mn_{0.7}$ (1565 ch) alloy has almost identical mechanical properties in the directions of 0°, 45°, and 90°, and the coefficient of planar anisotropy (generalized coefficient including $r_{0°}$, $r_{45°}$ and $r_{90°}$) is 0.87, which means an almost complete isotropy of properties (see Table 5). It can be assumed that the slight anisotropy that is still observed is associated with the remaining Bs texture.

Table 5. Mechanical properties of the Al $Mg_6Mn_{0.7}$ (1565 ch) alloy after annealing at 500 °C (1 h).

Direction to RD	$\sigma_{0,2}$ (MPa)	σ_u (MPa)	*A*%	*n*	Δ*r*
0°	160 ± 2	320 ± 3	24 ± 1	0.26 ± 0	
45°	158 ± 4	321 ± 3	25 ± 1	0.26 ± 0	0.87
90°	156 ± 4	321 ± 4	24 ± 1	0.25 ± 0	

Hence, due to the PSN mechanism it is possible to obtain an almost random texture and "textureless" properties close to isotropic in the $AlMg_6Mn_{0.7}$ (1565 ch) alloy. On the one hand, it is necessary to strive for the maximum possible Zener-Hollomon parameter during hot rolling in a continuous group (or reversible stand) in order to increase the number of PSN nuclei that appear on intermetallic particles and contribute to the development of a textureless (random) component during recrystallization. On the other hand, high Zener parameters require the temperature to be decreased (since the latter affects it more than the strain rate), which will facilitate no or only partial recrystallization. Thus, if hot deformation is the final stage of thermomechanical treatment, it must be carried out at high Zener parameters in order to obtain the maximum possible amount of textureless (random) component. However, the temperature should not drop below 350 °C since in this case complete recrystallization is impossible.

During the final annealing for one hour after cold rolling at a temperature equal to or greater than 350 °C, complete recrystallization can be observed in the $AlMg_6Mn_{0.7}$ (1565 ch) alloy. The textureless component (random texture) is formed and the material properties are close to being isotropic.

3.4. Computational Result

Figure 17 shows the computation of texture evolution of the Cube, β-fiber fraction from the Zener-Hollomon parameter which is directly determined by the deformation process temperature and rate [38].

$$Z = \dot{\varepsilon} exp\left(\frac{Q}{RT}\right) \quad (2)$$

where $\dot{\varepsilon}$ is strain rate, T is temperature, R is the molar gas constant and Q is the activation energy [J/mol].

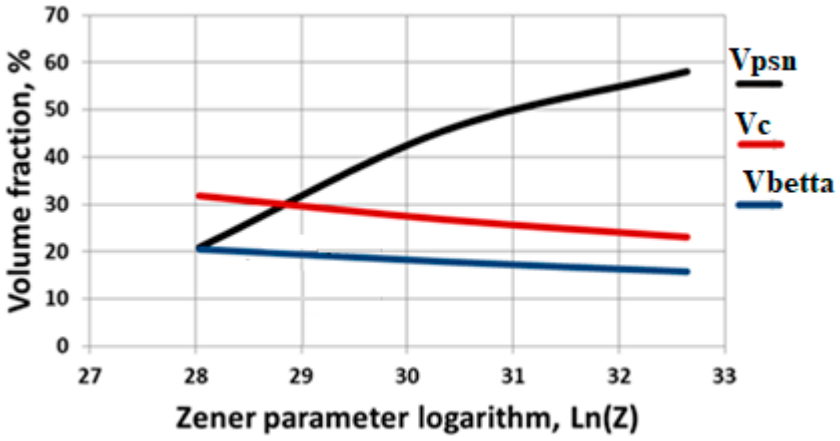

Figure 17. Result of simulation dependence of Cube, β–piber and PSN fraction volume from Zener-Hollomon parameter, with account for intermetallic particle refinement in the $AlMg_6Mn_{0.7}$ (1565 ch) alloy.

The β-fiber fractions consist of Bs, Cu, and S components. Euler angles and Miller indices of all these components as well as the Cube fraction are present in Table 6. Additionally, in Figure 8 the dependence of the PSN fraction from the Zener-Hollomon parameter are present. The PSN fraction consists of grain nucleated during recrystallization at second phase particles. As was mention before, grains which recrystallize by the PSN mechanism give a mostly random texture.

Table 6. Euler angles of Ideal texture components "β-fiber" according to [39].

Component	Miller Indices {hkl}⟨uvw⟩	Euler Angles		
		φ_1	Φ	φ_2
Cube	{001}⟨100⟩	0	0	0°/90
Bs	{011}⟨211⟩	35°	45°	0°/90°
Cu	{112}⟨111⟩	90°	30°	45°
S	{123}⟨634⟩	60°	35°	65°

Note that at a low Zener-Hollomon parameter value the subgrains of magnesium rich alloys have the same size as the subgrains of lean (low alloyed) aluminum alloys. Thus, at a low Zener parameter the nuclei formed from subgrains and second phase particles during hot rolling of the as-cast structure are comparable in size. Therefore, at low Zener-Hollomon parameter values the PSN-based recrystallized volume fraction is comparable in volume fractions with the cube texture and β-fiber texture. As the Zener-Hollomon parameter increases, the subgrain size decreases and the PSN-based recrystallized volume fraction grows-at the same time as the volume fractions of the cube and β-fiber textures decrease.

Recrystallization of $AlMg_6Mn_{0.7}$ (1565 ch) is quite complex during this stage of thermomechanical treatment due to the interdependence on classical and particle stimulated

recrystallization and the interaction with fine dispersoids, blocking grain boundary motion, and it requires a high Zener parameter [40]. Since recrystallization is needed for texture evolution and control in aluminum alloys, hot rolling such alloys in the reversing mill with a high Zener parameter value is a suitable approach. Some more random texture constituents will prevail after such hot rolling. In this alloy it has a positive effect, as it will reduce the β fiber texture fraction during the final stage of hot rolling. It shall be noted that for recrystallization of grains with a lower β fiber texture the mechanism of oriented growth is less pronounced, decreasing the cube texture volume fraction. The Zener parameter will be very high during the final stages of hot rolling, and the subgrain size will be very small. This is the reason why during recrystallization the PSN will successfully compete with the formation of the cube texture, even completely suppressing it in some cases [13]. The smaller the β fiber texture fraction is, the more efficiently the cube texture will be suppressed. Thus, a total absence of any pronounced texture is possible during the final stages of hot rolling. Following cold rolling completion and final recrystallization annealing, a microstructure can also be achieved in such an alloy, having no defined texture components, i.e., having a random texture.

Self-annealing simulations were carried out at different temperatures and different Zener-Hollomon parameters characteristic of hot rolling to explain this effect.

Figure 18 shows the dependences of the recrystallized volume, cube and random orientation (PSN) proportions on the Zener parameter for the $AlMg_6Mn_{0.7}$ (1565 ch) alloy obtained by simulation. Note that the temperature has a prevailing effect on the Zener parameter during rolling.

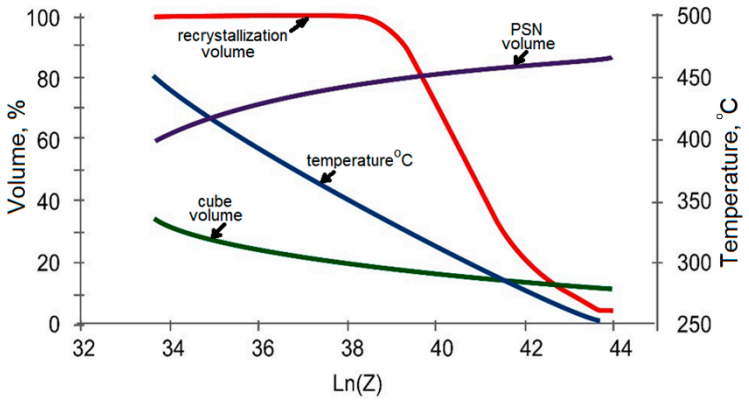

Figure 18. Dependences of the recrystallized volume, cube and random orientation (PSN) proportions on the Zener parameter for the $AlMg_6Mn_{0.7}$ (1565 ch) alloy obtained during simulation.

As can be seen from Figure 18, the β-texture is not formed at all since the sizes of its nuclei are too small and their development is suppressed by fine particles. The proportion of the cube texture is very small. Thus, the $AlMg_6Mn_{0.7}$ (1565ch) alloy is a material in which almost isotropic properties can be obtained by adjusting the annealing or self-annealing temperature. This method is based on the PSN mechanism. The insufficient temperature for recrystallization, which is shown in Figure 18, seems to be the only problem. The texture of this alloy is very sensitive to the hot rolling end (coil exit) temperature. It determines the temperature of self-annealing since the uncrystallized rolling (β-fiber) textures may prevail in this case, which will interfere with the cube and PSN texture, obtaining an isotropic (balanced) texture. In general, it is possible to obtain it at this stage.

It should also be noted that the Zener-Hollomon parameter and the number of PSN-nuclei participating in recrystallization increase when the temperature decreases. However, recrystallization takes place only partially at temperatures below 350 °C and it contributes to the preservation of the rolling (β-fiber) texture.

It is very important to get a fully recrystallized structure for control of the texture formation during the annealing process after cold deformation. In the absence of recrystal-

lization, a pronounced β-fiber texture [12] is formed. The possibility of recrystallization is directly affected by the driving P_d and the retarding P_z forces. The Equations (1) and (3) were used to calculate the driving and retarding recrystallization forces during the annealing process.

$$P_D = \frac{\rho G b^2}{2} \quad (3)$$

ρ is the dislocation density (taken as 10^{15} m^2 during cold deformation), G is the Young modulus of aluminum (taken 7 × 1012 N/m^2), and b is the abs. value of Burgers vector (taken 0.2 × 10^{-9}) [4].

It should be noted that the Equation (3) uses a somewhat simplified approach to calculating P_d. It suggests that the driving force of recrystallization is determined by the number of dislocations that are present in the cold-rolled metal. Nevertheless, dislocation density is not constant and some dislocations annihilate during the heating time. In this case, the workpiece thickness was several mm, and heating was carried out in a saltpeter bath. As a result the decrease in dislocation density can be neglected and the calculated value of P_D does not depend on the temperature. At 250 °C, the retarding force exceeds the driving force, so recrystallization does not occur (Figure 19). At 350 °C, some of the fine particles of the Mg_2Si type dissolve, so the P_D exceeds the P_z and as a result the recrystallization process occurs. When the temperature reaches 500 °C, the dark particles completely disappear, see Figure 9. This lead to a significant drop in the breaking force compared to the 350 °C case.

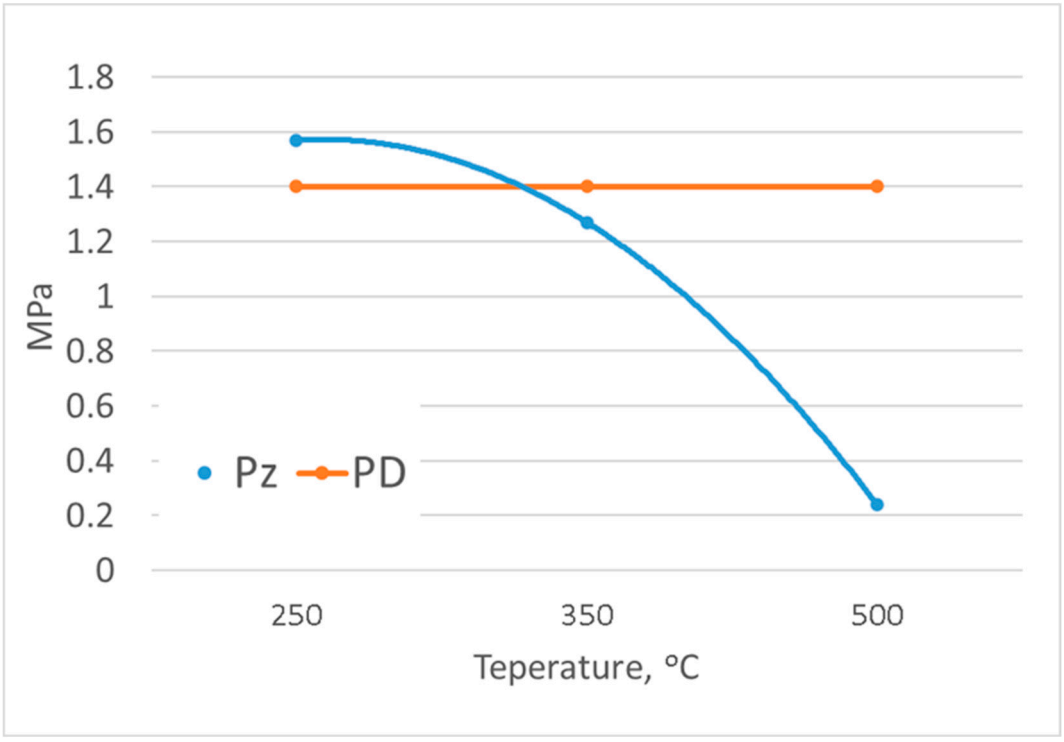

Figure 19. Dependence of the driving and retarding forces of recrystallization from the annealing temperature.

The critical particle radius of particles η^* is calculated, after which it become a recrystallization nucleus. To determine the quantity of particles which take part in the PSN mechanism, one substracts the number of particles which have a value of η^* less then critical.

$$\text{As } \eta^* = \frac{2\gamma_B}{P_D} \quad (4)$$

γ_B is the energy of a high angle boundary (taken 0.5 J m^{-2}).

The dependance of the number of particles capable for new grain nucleation from the annealing temperature is present in Figure 20. As can be seen, the number of participles which can become nuclei decreases with increasing temperature, since the total amount of intermetallics decreases due to the dissolution of large particles of the Mg_2Si type. However, it should be noted that despite the decrease in the total number of large intermetallic particles, the PSN mechanism is predominant. What can be seen from the results of the texture and mechanical properties analysis given earlier are shown in Figure 16 and Table 6. It should be noted that during self-annealing, the total amount of intermetallic that are suitable for nucleation is 2.5 × 10^{12}. In the case of annealing at 350 °C, the total number of particles 8 × 10^{13} is suitable nucleation. This could be explained by the fact that in the cold-deformed state, due to the higher dislocation density, the potential size for nucleation is much smaller than in the hot state. Therefore, despite the fact that the total number of particles during self-annealing is greater, the nuclei number is much less.

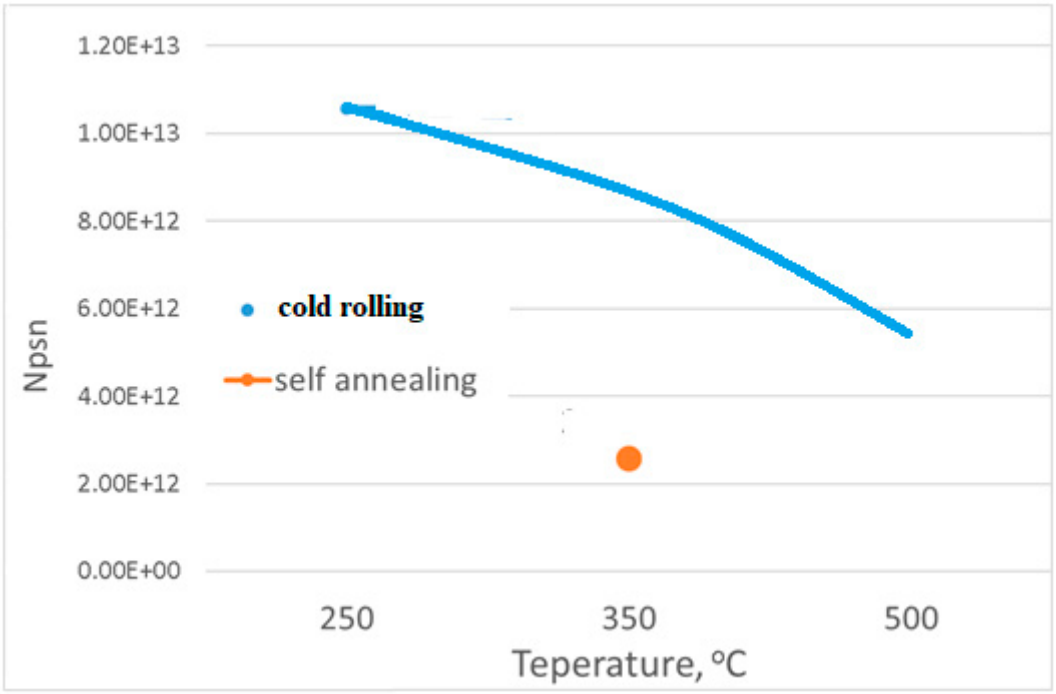

Figure 20. The amount of particles which can contribute to recrystallization (according to the driving and retarding forces for recrystallization and their dependence on the annealing temperature.

4. Conclusions

1. Recrystallization processes do not occur in the $AlMg_6Mn_{0.7}$ (1565 ch) alloy during the hot deformation of the cast structure. The dendritic as-cast structure is stretched in the rolling direction and the β-fiber texture is formed, in which the Bs-orientation plays a dominant role. Because of the rather low Zener-Hollomon parameters and the retarding effect from the second-phase fine particles, recrystallization does not occur in the experimentally investigated modes of hot working the as-cast structure. Modeling shows that the PSN mechanism will be the main nucleation mechanism during recrystallization as the Zener-Hollomon parameter increases.

2. When rolling in a continuous hot rolling group, recrystallization does not occur in the interstand space due to the fine second-phase particles and the short inter-pass times. As a result, further accumulation of plane strain rolling (β-fiber) orientations, mainly in the form of the development of S- and Cu-components, occurs. The $AlMg_6Mn_{0.7}$ (1565 ch) alloy is completely recrystallized during self-annealing after hot rolling. In this case, the main prevailing mechanism is particle stimulated nucleation "PSN" on intermetallic particles,

which leads to a significant volume of a random texture with small fragments of the cube texture. Modeling shows that the proportion of the random component increases as the temperature and the Zener-Hollomon parameters increase.

3. A pronounced texture of β-fiber with three classical components (Bs-, Cu- and S) is formed during cold rolling, but with the Bs component as the most pronounced. Recrystallization after cold rolling of the $AlMg_6Mn_{0.7}$ (1565 ch) alloy begins at a temperature of >>300 °C. After recrystallization during cold rolling, a random (textureless) component with a small proportion of Bs-textures is formed. Analysis of the mechanical properties shows almost complete isotropy.

Author Contributions: Conceptualization, E.A. and A.D.; methodology, J.H. and V.A.; software, E.A. and J.H.; validation, J.H., V.A. and A.D.; formal analysis, J.H.; investigation, E.A. and M.T.; resources, E.A., S.K. and V.A.; data curation, E.A.; writing—original draft preparation —E.A.; writing—review and editing —J.H., A.D.; visualization, M.T.; supervision, E.A.; project administration, E.A.; funding acquisition, E.A. All authors have read and agreed to the published version of the manuscript.

Funding: The study was supported by a grant from the Russian Science Foundation, project No. 18-79-10099-P, https://rscf.ru/en/project/21-79-03041/, accessed on 10 March 2022.

Data Availability Statement: The data presented in this study are available on request from the corresponding author.

Conflicts of Interest: The authors declare that they have no conflict of interest.

References

1. Chausov, M.G.; Berezin, V.B.; Pylypenko, A.P.; Hutsaylyuk, V.B. Strain field evolution on the surface of aluminum sheet alloys exposed to specific impact with oscillation loading. *J. Strain Anal. Eng. Des.* **2015**, *50*, 61–72. [CrossRef]
2. Chausov, M.; Maruschak, P.; Zasimchuk, E.; Pypypenko, A.; Bishchak, R.; Burda, I. About physical aspects of increasing durability of aluminum alloys due to impact-oscillatory loading. In *International Conference TRANSBALTICA: Transportation Science and Technology*; Springer: Cham, Switzerland, 2021; pp. 572–580. [CrossRef]
3. Savchenkov, S.; Kosov, Y.; Bazhin, V.; Krylov, K.; Kawalla, R. Microstructural Master Alloys Features of Aluminum–Erbium System. *Crystals* **2021**, *11*, 1353. [CrossRef]
4. Kosov, Y.I.; Bazhin, V.Y.; Povarov, V.G. Interaction of Erbium Fluoride with Alkali Metal Chloride–Fluoride Melts in Synthesizing an Al–Er Master Alloy. *Russ. Metall. (Metally)* **2018**, *6*, 539–544. [CrossRef]
5. Belov, N.A.; Alabin, A.N.; Sannikov, A.V.; Deev, V.B. Primary crystallization in the Al-Fe-Mn-Ni-Si system as applied to casting alloys based on aluminum-nickel eutectic. *Russ. J. Non-Ferr. Met.* **2014**, *55*, 356–364. [CrossRef]
6. Belov, N.A.; Akopyan, T.K.; Korotkova, N.O.; Timofeev, V.N.; Shurkin, P.K. Effect of cold rolling and annealing temperature on structure, hardness and electrical conductivity of rapidly solidified alloy of Al–Cu–Mn–Zr system. *Mater. Lett.* **2021**, *300*, 130199. [CrossRef]
7. Engler, O.; Kalz, S. Simulation of earing profiles from texture data by means of a visco-plastic self-consistent polycrystal plasticity approach. *Mater. Sci. Eng. A* **2004**, *373*, 350–362. [CrossRef]
8. Engler, O. Modeling of texture and texture-related properties during the thermo-mechanical processing of aluminum sheets. *Mater. Sci. Forum* **2003**, *426*, 3655–3660. [CrossRef]
9. Hutchinson, W.B.; Oscarsson, A.; Karlsson, Å. Control of microstructure and earing behaviour in aluminium alloy AA 3004 hot bands. *Mater. Sci. Technol.* **1989**, *5*, 1118–1127. [CrossRef]
10. Engler, O.; Hirsch, J. Polycrystal-plasticity simulation of six and eight ears in deep-drawn aluminum cups. *Mater. Sci. Eng. A* **2007**, *452*, 640–651. [CrossRef]
11. Engler, O. Control of texture and earing in aluminium alloy AA 3105 sheet for packaging applications. *Mater. Sci. Eng. A* **2012**, *538*, 69–80. [CrossRef]
12. Aryshenskii, E.V.; Hirsch, J.; Konovalov, S.V.; Prahl, U. Specific features of microstructural evolution during hot rolling of the as-cast magnesium-rich aluminum alloys with added transition metal elements. *Metall. Mater. Trans. A* **2019**, *50*, 5782–5799. [CrossRef]
13. Aryshenskii, E.V.; Aryshenskii, V.Y.; Beglov, E.D.; Chitnaeva, E.S.; Konovalov, S.V. Investigation of subgrain and fine intermetallic participles size impact on grain boundary mobility in aluminum alloys with transitional metal addition. *Mater. Today Proc.* **2019**, *19*, 2183–2188. [CrossRef]
14. Zaidi, M.A.; Sheppard, T. Development of microstructure throughout roll gap during rolling of aluminium alloys. *Met. Sci.* **1982**, *16*, 229–238. [CrossRef]
15. Vatne, H.E.; Wells, M.A. Modelling of the recrystallization behaviour of AA5XXX aluminum alloys after hot deformation. *Can. Metall. Q* **2003**, *42*, 79–88. [CrossRef]

16. Aryshenskii, E.; Kawalla, R.; Hirsch, J. Development of new fast algorithms for calculation of texture evolution during hot continuous rolling of Al–Fe alloys. *Steel Res. Int.* **2017**, *88*, 1700053. [CrossRef]
17. Evgenii, A.; Erkin, B.; Hirsch, J.; Vladimir, A.; Segrey, K. Development of the new fast approach for calculation of texture evolution during hot deformation of aluminum alloys. *Procedia Manuf.* **2019**, *37*, 492–499. [CrossRef]
18. Aryshenskii, E.; Hirsch, J.; Konovalov, S.; Aryshenskii, V.; Drits, A. Influence of mg content on texture development during hot plain-strain deformation of aluminum alloys. *Metals* **2021**, *11*, 865. [CrossRef]
19. Engler, O.; Miller-Jupp, S. Control of second-phase particles in the Al-Mg-Mn alloy AA 5083. *J. Alloy. Compd.* **2016**, *689*, 998–1010. [CrossRef]
20. Engler, O.; Kuhnke, K.; Hasenclever, J. Development of intermetallic particles during solidification and homogenization of two AA 5xxx series Al-Mg alloys with different Mg contents. *J. Alloy. Compd.* **2017**, *728*, 669–681. [CrossRef]
21. Tepterev, M.S.; Aryshenskii, E.V.; Guk, S.V.; Bazhenov, V.E.; Drits, A.M.; Kavalla, R. Effect of annealing conditions on the evolution of the grain structure and intermetallic phases in the cold-rolled strip of aluminum–magnesium alloy. *Phys. Met. Metallogr.* **2020**, *121*, 906–913. [CrossRef]
22. Gottstein, G. *Grain Boundary Migration in Metals: Thermodynamics, Kinetics, Applications*; CRC Press: Boca Raton, FL, USA, 1999.
23. Maire, E.; Grenier, J.C.; Daniel, D.; Baldacci, A.; Klöcker, H.; Bigot, A. Quantitative 3D characterization of intermetallic phases in an Al–Mg industrial alloy by X-ray microtomography. *Scr. Mater.* **2006**, *55*, 123–126. [CrossRef]
24. Moulin, N.; Parra-Denis, E.; Jeulin, D.; Ducottet, C.; Bigot, A.; Boller, E.; Klöcker, H. Constituent Particle Break-Up During Hot Rolling of AA 5182. *Adv. Eng. Mater.* **2010**, *12*, 20–29. [CrossRef]
25. Aryshenskii, E.; Hirsch, J.; Konovalov, S. Investigation of the intermetallic compounds fragmentation impact on the formation of texture during the as cast structure thermomechanical treatment of aluminum alloys. *Metals* **2021**, *11*, 507. [CrossRef]
26. Humphreys, F.J. The nucleation of recrystallization at second phase particles in deformed aluminium. *Acta Metall.* **1977**, *25*, 1323–1344. [CrossRef]
27. Hirsch, J.; Karhausen, K.; Kopp, R. Microstructure simulation during hot rolling of Al-Mg alloys. In Proceedings of the 4th International 1994 Conference on Aluminium Alloys (ICAA4), Atlanta, GA, USA, 11–16 September 1994.
28. Hirsch, J. Thermomechanical control in aluminium sheet production. *Mater. Sci. Forum* **2003**, *426*, 185–194. [CrossRef]
29. Hirsch, J.; Aryshesnkij, E.; Konovalov, S. Slip System Selection and Taylor Factor Evolution in FCC Metals. 2020, p. 3618715. Available online: https://papers.ssrn.com/sol3/papers.cfm?abstract_id=3618715 (accessed on 13 March 2022). [CrossRef]
30. Aryshenskii, E.V.; Aryshenskii, V.Y.; Grechnikova, A.F.; Beglov, E.D. Evolution of texture and microstructure in the production of sheets and ribbons from aluminum alloy 5182 in modern rolling facilities. *Met. Sci. Heat Treat.* **2014**, *56*, 347–352. [CrossRef]
31. Wells, M.A.; Samarasekera, I.V.; Brimacombe, J.K.; Hawbolt, E.B.; Lloyd, D.J. Modeling the microstructural changes during hot tandem rolling of AA5XXX aluminum alloys: Part I. Microstructural evolution. *Metall. Mater. Trans. B* **1998**, *29*, 611–620. [CrossRef]
32. Humphreys, F.J.; Hatherly, M. *Recrystallization and Related Annealing Phenomena*; Elsevier: Amsterdam, The Netherlands, 2012.
33. Randle, V.; Engler, O. *Introduction to Texture Analysis: Macrotexture, Microtexture and Orientation Mapping*; CRC Press: Boca Raton, FL, USA, 2000.
34. Liu, W.C.; Zhai, T.; Morris, J.G. Comparison of recrystallization and recrystallization textures in cold-rolled DC and CC AA 5182 aluminum alloys. *Mater. Sci. Eng. A* **2003**, *358*, 84–93. [CrossRef]
35. Engler, O. Through-process modelling of the impact of intermediate annealing on texture evolution in aluminium alloy AA 5182. *Model. Simul. Mater. Sci. Eng.* **2003**, *11*, 863. [CrossRef]
36. Hirsch, J. Texture evolution during rolling of aluminum alloys. In *Light Metals-Warrendale-Proceedings*; TMS: Pittsburgh, PA, USA, 2008; p. 1071.
37. Rushchits, S.V.; Aryshenskii, E.V.; Kawalla, R.; Serebryany, V. Investigation of texture structure and mechanical properties evolution during hot deformation of 1565 aluminum alloy. *Mater. Sci. Forum* **2016**, *854*, 73–78. [CrossRef]
38. Zener, C.; Hollomon, J.H. Effect of strain rate upon plastic flow of steel. *J. Appl. Phys.* **1944**, *15*, 22–32. [CrossRef]
39. Engler, O.; Hirsch, J.; Lücke, K. Texture development in Al-1.8 wt% Cu depending on the precipitation state—II. Recrystallization textures. *Acta Metall. Mater.* **1995**, *43*, 121–138.
40. Yashin, V.; Aryshenskii, E.; Hirsch, J.; Konovalov, S.; Latushkin, I. Study of recrystallization kinetics in AA5182 aluminium alloy after deformation of the as-cast structure. *Mater. Res. Express* **2019**, *6*, 066552. [CrossRef]